Toward a General Theory of Hydrogen Bonding: The Short, Strong Hydrogen Bond [HOH⊙⊙⊙OH]−

ARTICLE *in* THE JOURNAL OF PHYSICAL CHEMISTRY A · OCTOBER 2000

Impact Factor: 2.69 · DOI: 10.1021/jp002726n

2 AUTHORS, INCLUDING:

Jan Halborg Jensen
University of Copenhagen
116 PUBLICATIONS **6,547** CITATIONS

Toward a General Theory of Hydrogen Bonding: The Short, Strong Hydrogen Bond $[HOH\cdots OH]^-$

Lynne C. Remer and Jan H. Jensen*

Department of Chemistry, University of Iowa, Iowa City, Iowa 52242

Received: July 31, 2000

The method of localized charge distributions is used to analyze the difference in hydrogen bond strength between $HOH\cdots OH_2$ and $[HOH\cdots OH]^-$ in terms of the competition between the electronic kinetic energy and potential energy. The main source of the difference is the relatively larger decrease in the intermolecular energy for the latter complex, due to the net charge and a more polar accepting lone pair. The decrease is interpreted semiquantitatively by using bond and lone pair dipoles. The shortening of the OO distance and the lengthening of the donating O−H bond are both shown to occur as a result of the stronger attraction. Implications for other short strong hydrogen bonds are discussed.

I. Introduction

Hydrogen bond (HB) strengths span a range of roughly 1−40 kcal/mol.[1] Much attention has been focused on HBs in the higher end of this range, since it was postulated that such bonds form within certain enzyme active sites and thus provide enough energy to explain the large rate enhancements associated with these remarkable catalysts.[2,3] This theory is not universally accepted,[4−6] and it is difficult to verify the theory by directly measuring the strengths of hydrogen bonds within enzyme active sites. The current, more indirect, approaches can be divided into two categories: (1) the study of the general *requirements* for strong HB formation and (2) the study of the properties or *characteristics* of strong HBs.

Some requirements mentioned frequently include:

(A) A relatively short distance between the two heteroatoms, usually taken to be <2.5 Å for O−H···O and O−H···N HBs.[1] This is a necessary but not sufficient requirement in the sense that a strong HB cannot form unless the heteroatoms are allowed to approach this closely. However, it does not mean that the HB strength can be increased simply by decreasing the heteroatom distance, since forcing this distance below its equilibrium value can only weaken a HB (as long as the nature of the donor and acceptor is not changed).[6] Thus, in the absence of any structural constraints, the short heteroatom distance is a *characteristic* of strong HBs, which are often referred to as short, strong hydrogen bonds (SSHBs).

(B) A relatively nonpolar environment. Both experimental[7] and computational[6,8] studies of SSHBs in different solvents indicate that the strength of SSHBs decrease rapidly as the polarity of the surrounding medium increases. The experimental estimates of the HB strength-decrease tend to be more severe than the computational estimates, but either estimate may not relate directly to the heterogeneous environment of an enzyme active site. However, a recent computational study by Mulholland, Lyne, and Karplus[9] has shown evidence of a decrease in SSHB strength (relative to the gas-phase value) due to the protein environment for citrate synthase.

(C) Identical pK_a (or proton affinity in the gas phase) of the two hydrogen bonded molecules. It has been suggested[2] that the strongest SSHB, $[A-H\cdots B]^-$, is formed when the pK_a of A^- and B^- are identical. The rationale is that the equal pK_a's allow the A−H and H−B bonds to lengthen and shorten, respectively, thereby increasing the covalent character of the H···B bond. Such bonds have a low barrier to proton transfer, and are therefore referred to as low barrier hydrogen bonds (LBHBs). This unusual bonding in LBHBs could then account for the extremely large low field proton shifts observed, another characteristic of LBHBs.[10] Indeed, a computational study by Kumar and McAllister[11] has demonstrated a linear relationship between proton shift and hydrogen bond strength.

Several experimental[7] and computational studies[8,12] have demonstrated a linear relationship between the increase in HB strength and the decrease in the difference in pK_a (ΔpK_a). However, the HB strengths for Δp$K_a = 0$ are not especially strong, so that any covalent contribution must increase gradually as ΔpK_a tends to zero. Furthermore, Herschlag[7] has observed that a simple electrostatic model is sufficient to explain the linear correlation.

It is important to note that the relationship between HB strength and ΔpK_a is, in general, only approximately linear and that the deviation from linearity increases as the hydrogen donor and acceptor become very different. So while the best hydrogen acceptor for A−H may be A^- [13] it is not *generally* possible to predict the relative strength of $[A-H\cdots B_1]^-$ and $[A-H\cdots B_2]^-$ based on the ΔpK_a's of B_1 and B_2 relative to A. For example, the gas-phase HB strength of $[HO-H\cdots OCH_3]^-$ (19.9 kcal/mol) is smaller than that of $[HO-H\cdots F]^-$ (23.3 kcal/mol) even though the ΔPA is smaller in the former system (9.3 kcal/mol) than in the latter (19.4 kcal/mol).[14] So, while a pK_a match is, by definition, necessary for a LBHB it is not necessary for a SSHB. Furthermore, the pK_a match criterion cannot be used to predict the relative strengths of, for example, $[HO-H\cdots OH]^-$ and $[Cl-H\cdots Cl]^-$.

The goal of the present study is develop a *conceptual understanding* of the large increase in HB strength on going from $HOH\cdots OH_2$ to $[HOH\cdots OH]^-$, to help account for and predict the relative strengths of SSHBs and elucidate their relationship to "conventional" HBs. The conceptual framework of our model is that pioneered by Ruedenberg[15,16] for covalent bonding: the competition between the kinetic energy pressure and the nuclear suction, which tend to favor expansion and contraction of the electron density, respectively. The study is

* Corresponding author: jan-jensen@uiowa.edu..

10.1021/jp002726n CCC: $19.00
Published on Web 09/13/2000

therefore not intended to directly address the relative importance of covalent and electrostatic interactions. The interplay between kinetic and potential energy is extracted by a careful analysis of hydrogen bond strengths using the theory of localized charge distributions.[17,18] The study is part of our efforts to understand the physical origins of hydrogen bonds in general.[18−20]

The paper is organized as follows. First, the theory of localized charge distributions (LCDs) is reviewed, together with two conceptually useful treatments of the electronic kinetic energy and intermolecular LCD energy terms. Second, previous applications of the LCD method to hydrogen bonding are briefly reviewed. Third, new results for $[HOH\cdots OH]^-$ are presented. Finally, the results are summarized and the general implications of our findings are discussed.

II. Theory

A. Localized Charge Distributions. A localized charge distribution[17,18] (LCD) consists of two parts: (1) a localized molecular orbital (LMO, ψ_i) and (2) its assigned local nuclear charge distribution [Z_i(A) for all atoms A]. A neutral molecule with N electrons in $N/2$ orbitals can be partitioned into $N/2$ LCDs by setting

$$\begin{aligned} Z_i(\mathrm{A}) &= 2 \text{ if } \psi_i \text{ is an inner-shell (core) or lone pair LMO predominantly localized on atom A} \\ &= 1 \text{ if } \psi_i \text{ is bond LMO predominantly localized on atom A and its bonded partner} \\ &= 0 \text{ otherwise} \end{aligned} \tag{1}$$

A prototypical example is the H_2O molecule. This molecule has 10 electrons in five doubly occupied *canonical* MOs. These MOs can then be energy localized using the Edmiston−Ruedenberg method[21] to give a core, two lone pair, and two bond LMOs. These five LMOs can then be used to define the local nuclear charge distributions: core and lone pair LMOs are assigned +2 charges positioned on the *one* atom (O) on which they are localized, whereas the bond LMOs are assigned +1 charges on each of the *two* atoms (O and H) on which they are localized.

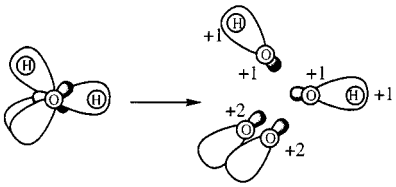

The charge partitioning scheme presented in eq 1 does not apply to charged species such as OH^- without modification. In the case of OH^- we treat the core and bond LCDs in the usual fashion, but assign a +5/3 charge to each of the lone pairs.

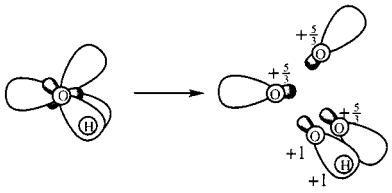

This approach has worked well in a previous study on the glycine zwitterion.[22]

In all cases, these assignments preserve the total nuclear charge on atom A (Z_A):

$$\sum_i Z_i(\mathrm{A}) = Z_\mathrm{A} \tag{2}$$

The three types of localized charge distributions illustrated for H_2O and OH^- can be used to describe all of the systems in this study. More complicated molecular systems require a more complicated nuclear charge partitioning as discussed previously.[18]

B. Total Energy Partitioning. *1. SCF Energy Partitioning.* Once the Z_i(A)'s are defined for a particular system it is possible to partition the total molecular SCF energy,

$$\begin{aligned} E^{\mathrm{SCF}} = &\sum_i \int \mathrm{d}\mathbf{r}\, \psi i(\mathbf{r}) \left[-\frac{1}{2}\nabla^2\right] \psi_i(\mathbf{r}) + \sum_i \int \mathrm{d}\mathbf{r}\, \psi_i(\mathbf{r}) \\ &[\sum_\mathrm{A} Z_\mathrm{A} R_\mathrm{A}^{-1}] \psi_i(\mathbf{r}) + \sum_i \sum_j \int\int \mathrm{d}\mathbf{r}_1\, \mathrm{d}\mathbf{r}_2\, [2|\psi_i(\mathbf{r}_1)|^2 |\psi_j(\mathbf{r}_2)|^2 - \\ &\psi_i(\mathbf{r}_1)\, \psi_j(\mathbf{r}_1)\, \psi_i(\mathbf{r}_2)\, \psi_j(\mathbf{r}_2)] r_{12}^{-1} + \sum_\mathrm{A} \sum_\mathrm{B} Z_\mathrm{A} Z_\mathrm{B} R_{\mathrm{AB}}^{-1} \end{aligned} \tag{3}$$

into localized contributions, by substituting eq 2 into eq 3,

$$\begin{aligned} E^{\mathrm{SCF}} &= \sum_i [T_i + \sum_j (V_{ij} + G_{ij} + g_{ij})] \\ &= \sum_i [T_i + \sum_j v_{ij}] \end{aligned} \tag{4}$$

where T, V, G, and g represent the electronic kinetic, electron−nuclear attraction, electron−electron repulsion, and nuclear−nuclear repulsion energies, respectively, due to each LCD or LCD pair. Explicit expressions for V_{ij} and g_{ij}, as well as a similar expression for the high spin ROHF energy can be found in ref 18.

2. MP2 Energy Partitioning. In this study, electron correlation is computed using second-order Møller−Plesset perturbation theory (MP2) within the frozen core approximation.[23] The MP2 energy correction is cast in terms of canonical valence pair energies,

$$E^{(2)} = \sum_i \sum_j e_{ij}^{(2)}$$

where

$$e_{ij}^{(2)} = \sum_r^{\mathrm{vir}} \sum_s^{\mathrm{vir}} C_{ij}^{\mathrm{rs}} \int\int \mathrm{d}\mathbf{r}_1\, \mathrm{d}\mathbf{r}_2\, \psi_i(\mathbf{r}_1)\, \psi_r(\mathbf{r}_1) r_{12}^{-1} \psi_j(\mathbf{r}_2)\, \psi_s(\mathbf{r}_2) \tag{5}$$

and included in the LCD analysis after separately transforming the integrals and coefficients using the same unitary transformation that transforms the canonical valence MOs to the LMO basis.[24]

$$\begin{aligned} E &= E^{\mathrm{SCF}} + E^{(2)} \\ &= \sum_i [T_i + \sum_j v_{ij} + \sum_j e_{ij}^{(2)}] \end{aligned} \tag{6}$$

This transformation leaves $E^{(2)}$ invariant and it is now composed of correlation energy contributions ($e_{ij}^{(2)}$) due to pairs of electrons in valence LMOs i and j.

C. Electronic Kinetic Energy. The electronic kinetic energy (KE) is of prime importance in our analysis, and this section summarizes a qualitative relation between the KE and the electron distribution. A more detailed discussion can be found in ref 20.

Levine[25] has pointed out that, since the momentum $\langle p_x \rangle = 0$ for stationary states, $(\Delta p_x)^2 = 2T_x$ for an electron and the uncertainty principle

$$(\Delta p_x)^2(\Delta x)^2 \geq \frac{1}{4} \tag{7}$$

yields an inverse relation between the square of the uncertainty of the electronic position (the second central moment or variance) and the KE,

$$T_x \geq \frac{1}{8(\Delta x)^2} \tag{8}$$

In the general case we assert that the *total* KE of a MO (i) is inversely proportional to its second central moment, so that a KE *change* can be related to the change in the reciprocal second moment (where $\langle r^2 \rangle = \langle x^2 \rangle + \langle y^2 \rangle + \langle z^2 \rangle$),

$$T_{i,\mathrm{A}} - T_{i,\mathrm{B}} \propto \left(\frac{1}{\langle r_{i,\mathrm{A}}{}^2 \rangle} - \frac{1}{\langle r_{i,\mathrm{B}}{}^2 \rangle} \right) \tag{9}$$

An important implication of this relation is the fact that identical changes in the second moment of two MOs $[\langle r_{1,\mathrm{A}}{}^2 \rangle - \langle r_{1,\mathrm{B}}{}^2 \rangle = \langle r_{2,\mathrm{A}}{}^2 \rangle - \langle r_{2,\mathrm{B}}{}^2 \rangle]$ will lead to a *larger* KE change for the more contracted MO. In this paper, we use this relation to relate the KE changes of different orbitals to changes in orbital size.

D. Multipole Representation of the Electrostatic Potential of LCDs. The electrostatic potential (V^{EP}) due to a LCD can be expanded in terms of multipoles just like any other charge distribution. In previous studies[18−20,22] we have taken advantage of this fact by modeling the interaction energy of relatively distant LCDs as multipole interactions. Since the charge distribution of LCDs are not very complex, only one or two multipole terms suffice for a semiquantitative description and it is relatively easy to develop a physical intuition about the magnitude and orientation of these multipoles in molecules and molecular complexes. We formalize our previous multipole treatments in the next two subsections and introduce a new multipole treatment for charged lone pairs in the third subsection.

1. Neutral Lone Pair LCDs. Previous studies[18−20,22] have shown that a single dipole, centered at the LMO centroid of charge, gives a good description of the V^{EP} of a neutral lone pair LCD.

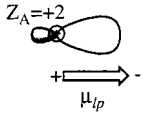

This amounts to a one-center expansion (around local origin $\mathbf{R}_{\mathrm{O}}$) of the V^{EP} (at point C due to a lone pair on nucleus A) followed by a truncation after the second term (the first term vanishes):

$$V_{\mathrm{lp}}^{\mathrm{EP}}(C) = -\int \mathrm{d}\mathbf{r}_1 \frac{\rho_{\mathrm{lp}}(\mathbf{r}_1)}{r_{1\mathrm{C}}} + \frac{2}{R_{\mathrm{AC}}} \qquad \text{where}$$

$$\rho_{\mathrm{lp}}(\mathbf{r}_1) = 2|\psi_{\mathrm{lp}}(\mathbf{r}_1)|^2$$

$$= [-\int \mathrm{d}\mathbf{r}_1\, \rho_{\mathrm{lp}}(\mathbf{r}_1) + 2]R_{\mathrm{OC}}{}^{-1} - [(-\int \mathrm{d}\mathbf{r}_1\, \rho_{\mathrm{lp}}(\mathbf{r}_1)\mathbf{r}_1 + 2\mathbf{R}_{\mathrm{A}})]R_{\mathrm{OC}}R_{\mathrm{OC}}{}^{-3} + \cdots$$

$$\approx -(\boldsymbol{\mu}_{\mathrm{lp}} \cdot \mathbf{R}_{\mathrm{OC}})R_{\mathrm{OC}}{}^{-3} \tag{10}$$

Thus, the lone pair LCD dipole is simply twice the distance between the LMO centroid of charge from the nucleus containing the lone pair. One would therefore expect, for example, the dipole of a fluorine lone pair to be *smaller* than for an oxygen lone pair (due to the larger nuclear charge on F) and hence predict a *weaker* interaction with another distant LCD. It is important to note that $\boldsymbol{\mu}_{\mathrm{lp}}$ is independent of the origin of expansion since it is derived from a neutral charge distribution.

2. Neutral Bond LCDs. A bond LCD is a slightly more complicated charge distribution and does therefore in general require one more multipole term for an adequate representation of its V^{EP}. Jensen and Gordon[18] initially proposed a one-center expansion of $V_{\mathrm{bo}}^{\mathrm{EP}}$(due to a bond between atoms A and B) truncated after the third term:

$$V_{\mathrm{bo}}^{\mathrm{EP}}(C) = -\int \mathrm{d}\mathbf{r}_1 \frac{\rho_{\mathrm{bo}}(\mathbf{r}_1)}{r_{1\mathrm{C}}} + \frac{1}{R_{\mathrm{AC}}} + \frac{1}{R_{\mathrm{BC}}}$$

$$\approx [-\int \mathrm{d}\mathbf{r}_1\, \rho_{\mathrm{bo}}(\mathbf{r}_1) + 1 + 1]R_{\mathrm{OC}}{}^{-1} - [(-\int \mathrm{d}\mathbf{r}_1\, \rho_{\mathrm{bo}}(\mathbf{r}_1)\mathbf{r}_1 + \mathbf{R}_{\mathrm{A}} + \mathbf{R}_{\mathrm{B}})] \cdot \mathbf{R}_{\mathrm{OC}}R_{\mathrm{OC}}{}^{-3} + \left[\left(-\frac{1}{2}\int \mathrm{d}\mathbf{r}_1\, \rho_{\mathrm{bo}}(\mathbf{r}_1)(3\mathbf{r}_1\mathbf{r}_1 - r_1{}^2\mathbf{I}) + \frac{1}{2}(3\mathbf{R}_{\mathrm{A}}\mathbf{R}_{\mathrm{A}} - R_{\mathrm{A}}{}^2\mathbf{I}) + \frac{1}{2}(3\mathbf{R}_{\mathrm{B}}\mathbf{R}_{B} - R_{\mathrm{B}}{}^2\mathbf{I})\right)\frac{1}{3}(3\mathbf{R}_{\mathrm{OC}}\mathbf{R}_{\mathrm{OC}} - R_{\mathrm{OC}}{}^2\mathbf{I})R_{\mathrm{OC}}{}^{-5} - \cdots$$

$$\approx -(\boldsymbol{\mu}_{\mathrm{bo}} \cdot \mathbf{R}_{\mathrm{OC}})R_{\mathrm{OC}}{}^{-3} + \frac{1}{3}\boldsymbol{\Theta}_{\mathrm{bo}}(3\mathbf{R}_{\mathrm{OC}}\mathbf{R}_{\mathrm{OC}} - R_{\mathrm{OC}}{}^2\mathbf{I})R_{\mathrm{OC}}{}^{-5} \tag{11}$$

Though adequate as a qualitative model of LCD interactions involving bonds, it is hard to extract physical insight or develop predictive powers from the quadrupole. For example, though a FH bond LCD is more polar than an OH bond LCD (in a water molecule), the FH bond quadrupole is smaller. This is a serious deficiency as the main motivation behind the multipole analysis is physical insight and intuition.

The need for the quadrupole moment term can be eliminated by performing a distributed two-center expansion (around local origins $\mathrm{O_A}$ and $\mathrm{O_B}$) instead,

$$V_{\mathrm{bo}}^{\mathrm{EP}}(C) = -\int \mathrm{d}\mathbf{r}_1 \frac{\rho_{\mathrm{bo}}(\mathbf{r}_1)}{r_{1\mathrm{C}}} + \frac{1}{R_{\mathrm{AC}}} + \frac{1}{R_{\mathrm{BC}}}$$

$$= \left\{-\frac{1}{2}\int \mathrm{d}\mathbf{r}_1 \frac{\rho_{\mathrm{bo}}(\mathbf{r}_1)}{r_{1\mathrm{C}}} + \frac{1}{R_{\mathrm{AC}}}\right\} + \left\{-\frac{1}{2}\int \mathrm{d}\mathbf{r}_1 \frac{\rho_{\mathrm{bo}}(\mathbf{r}_1)}{r_{1\mathrm{C}}} + \frac{1}{R_{\mathrm{BC}}}\right\}$$

$$\approx \left\{\left[-\frac{1}{2}\int \mathrm{d}\mathbf{r}\, \rho_{\mathrm{bo}}(\mathbf{r}_1) + 1\right]R_{\mathrm{O_AC}}{}^{-1} - \left[\left(-\frac{1}{2}\int \mathrm{d}\mathbf{r}\, \rho_{\mathrm{bo}}(\mathbf{r}_1)\mathbf{r}_1 + \mathbf{R}_{\mathrm{A}}\right)\right] \cdot \mathbf{R}_{\mathrm{O_AC}}R_{\mathrm{O_AC}}{}^{-3} + \cdots + \left\{\left[-\frac{1}{2}\int \mathrm{d}\mathbf{r}\, \rho_{\mathrm{bo}}(\mathbf{r}_1) + 1\right]R_{\mathrm{O_BC}}{}^{-1} - \left[\left(-\frac{1}{2}\int \mathrm{d}\mathbf{r}\, \rho_{\mathrm{bo}}(\mathbf{r}_1)\mathbf{r}_1 + \mathbf{R}_{\mathrm{B}}\right)\right] \cdot \mathbf{R}_{\mathrm{O_BC}}R_{\mathrm{O_BC}}{}^{-3} + \cdots$$

$$\approx -(\boldsymbol{\mu}_{\mathrm{bo,A}} \cdot \mathbf{R}_{\mathrm{O_AC}})R_{\mathrm{O_AC}}{}^{-3} - (\boldsymbol{\mu}_{\mathrm{bo,B}} \cdot \mathbf{R}_{\mathrm{O_BC}})R_{\mathrm{O_BC}}{}^{-3} \tag{12}$$

Since each multipole expansion now describes a simpler charge distribution it can be truncated after the dipole, rather than the

quadrupole, without loss of accuracy.[20] More importantly, the polarity of the bond is now easily visualized in terms of the relative lengths of $\boldsymbol{\mu}_{\mathrm{bo,A}}$, since $\boldsymbol{\mu}_{\mathrm{bo,B}}$. Again, since $\boldsymbol{\mu}_{\mathrm{bo,A}}$ and $\boldsymbol{\mu}_{\mathrm{bo,B}}$

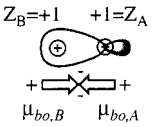

are derived from neutral charge distributions they are independent of origin. In this study we place the two origins at the respective geometric midpoint between the centroid of charge and the nucleus.

3. Charged Lone Pair LCDs. In this study, the negative charge on the anionic systems is divided equally among the lone pairs on OH^- by assigning to them a $+5/3$ nuclear charge, rather than the full $+2$ charge prescribed by eq 1. Thus, a monopole term has to be added to the multipole expansion. However, in a one center expansion,

$$\begin{aligned} V_{\mathrm{lp}^-}^{\mathrm{EP}}(C) &= -\int \mathrm{d}\mathbf{r}_1 \frac{\rho_{\mathrm{lp}}(\mathbf{r}_1)}{r_{1\mathrm{C}}} + \frac{5/3}{R_{\mathrm{AC}}} \\ &\approx [-\int \mathrm{d}\mathbf{r}_1\, \rho_{\mathrm{lp}}(\mathbf{r}_1) + {}^5/_3]R_{\mathrm{OC}}{}^{-1} - \\ &\qquad [(-\int \mathrm{d}\mathbf{r}_1\, \rho_{\mathrm{lp}}(\mathbf{r}_1)\mathbf{r}_1 + {}^5/_3\mathbf{R}_{\mathrm{A}})]\cdot \\ &\qquad\qquad \mathbf{R}_{\mathrm{OC}}R_{\mathrm{OC}}{}^{-3} + \cdots \\ &\approx -{}^1/_3 R_{\mathrm{OC}}{}^{-1} - (\boldsymbol{\mu}_{\mathrm{lp}}{}'\cdot\mathbf{R}_{\mathrm{OC}})R_{\mathrm{OC}}{}^{-3} \end{aligned} \tag{13}$$

the dipole is now origin dependent and not a simple function of the nuclear-centroid of charge separation. Thus, such a multipole expansion does not facilitate a direct comparison, for example, between charged and neutral lone pair LCDs. A repartitioning of the nuclear charge, similar to the repartitioning of the electronic charge for the bond, removes these undesirable features:

$$\begin{aligned} V_{\mathrm{lp}^-}^{\mathrm{EP}}(C) &= -\int \mathrm{d}\mathbf{r}_1 \frac{\rho_{\mathrm{lp}}(\mathbf{r}_1)}{r_{1\mathrm{C}}} + \frac{5/3}{R_{\mathrm{AC}}} \\ &= -\int \mathrm{d}\mathbf{r}_1 \frac{\rho_{\mathrm{lp}}(\mathbf{r}_1)}{r_{1\mathrm{C}}} + \frac{2}{R_{\mathrm{AC}}} + \frac{-1/3}{R_{\mathrm{AC}}} \\ &\approx \frac{-1/3}{R_{\mathrm{AC}}} + [-\int \mathrm{d}\mathbf{r}_1\, \rho_{\mathrm{lp}}(\mathbf{r}_1) + 2]R_{\mathrm{OC}}{}^{-1} - \\ &\qquad [(-\int \mathrm{d}\mathbf{r}_1\, \rho_{\mathrm{lp}}(\mathbf{r}_1)\mathbf{r}_1 + 2\mathbf{R}_{\mathrm{A}})]\cdot\mathbf{R}_{\mathrm{OC}}R_{\mathrm{OC}}{}^{-3} + \cdots \\ &\approx \frac{-1/3}{R_{\mathrm{AC}}} - (\boldsymbol{\mu}_{\mathrm{lp}}\cdot\mathbf{R}_{\mathrm{OC}})R_{\mathrm{OC}}{}^{-3} \end{aligned} \tag{14}$$

We have found that both representations of the electrostatic potential model inter-LCD interaction energies equally well. But for the latter expansion the dipole is origin-independent and can be directly compared to a corresponding neutral LCD dipole, since it is a measure of the same physical phenomenon. Thus, we use this expansion throughout.

III. Energy Decomposition Using LCDs

The LCD method has been used to analyze hydrogen bonds in both the neutral water dimer[18,19] and water−HF[20] complexes, and this study builds upon the results of those papers. Figure 1 shows that the total energy of the two approaching water molecules in the water dimer can be viewed as arising from

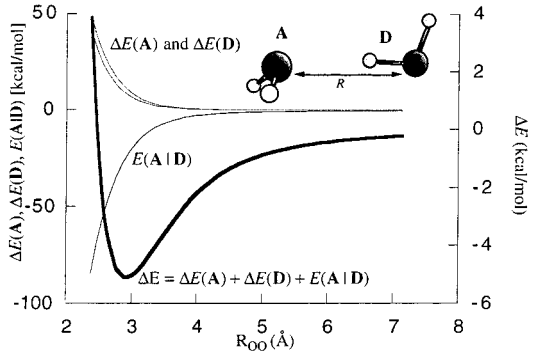

Figure 1. Change in the total (bold, right *y*-axis), internal, and intermolecular energies (eq 15) of water dimer relative to two free waters and as a function of OO separation.

two competing contributions: the increasing internal energies of the donor and acceptor molecules and their decreasing intermolecular energy [$E(\mathbf{A}|\mathbf{D})$] defined here,

$$\begin{aligned} \Delta E &= E(\mathbf{A}) + E(\mathbf{D}) + E(\mathbf{A}|\mathbf{D}) - [E_{\mathbf{A}} + E_{\mathbf{D}}] \\ &= [E(\mathbf{A}) - E_{\mathbf{A}}] + [E(\mathbf{D}) - E_{\mathbf{D}}] + E(\mathbf{A}|\mathbf{D}) \\ &= \Delta E(\mathbf{A}) + \Delta E(\mathbf{D}) + E(\mathbf{A}|\mathbf{D}) \end{aligned} \tag{15}$$

Here $E_{\mathbf{A}}$ and $E_{\mathbf{D}}$ are the energies of the isolated acceptor and donor molecules, respectively, while the intra- and intermolecular energies are obtained by restricting the summation in eq 6,

$$E(\mathbf{A}) = \sum_{i\in\mathbf{A}}[T_i + \sum_{j\in\mathbf{A}} v_{ij} + \sum_{j\in\mathbf{A}} e_{ij}^{(2)}] \tag{16}$$

$$E(\mathbf{D}) = \sum_{i\in\mathbf{D}}[T_i + \sum_{j\in\mathbf{D}} v_{ij} + \sum_{j\in\mathbf{D}} e_{ij}^{(2)}] \tag{17}$$

$$E(\mathbf{A}|\mathbf{D}) = \sum_{i\in\mathbf{A}}\sum_{j\in\mathbf{A}}[\sum_{j\in\mathbf{D}} 2v_{ij} + \sum_{j\in\mathbf{D}} 2e_{ij}^{(2)}] \tag{18}$$

The internal energy increase (from the variational minimum at infinite separation) results from the electronic kinetic energy increase due to contraction of select LMOs. For **D** it is the bond LMO involved in the hydrogen bond ($\mathrm{bo}'_{\mathbf{D}}$). For **A** it is all valence LMOs except the accepting lone pair ($\mathrm{lp}'_{\mathbf{A}}$) at OO distances larger than equilibrium, but as the OO distance is decreased further the expansion of $\mathrm{lp}'_{\mathbf{A}}$ is reversed (to satisfy the Pauli exclusion principle) and the associated energy increase dominates. Thus, Pauli (steric)[26] repulsion is an important factor at equilibrium hydrogen bond distances.

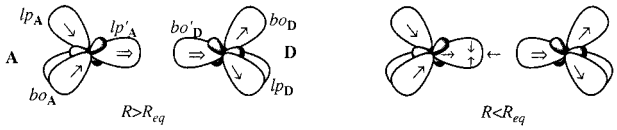

Interestingly, when the hydrogen donor is changed from H_2O to HF the hydrogen bond strength increases because the internal energy of HF *increases at a slower rate* than for H_2O.[20] *Thus, the forces that hold the two molecules together are not necessarily the forces that determine the difference in donor or acceptor ability.*

IV. Computational Methodology

The geometries of H_2O, OH^-, $(H_2O)_2$, and $[HOH\cdots OH]^-$ were fully optimized (within C_{2v}, $C_{\infty v}$, C_s, and C_1 symmetries,

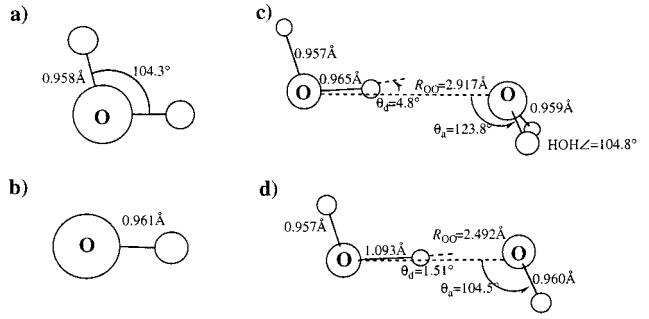

Figure 2. Fully optimized MP2/6-311++G(2d,2p) structures of (a) H_2O, (b) OH^-, (c) $(H_2O)_2$ (structure I, Scheme 1), and (d) $[HOH\cdots OH]^-$ (structure V, Scheme 1).

respectively) using second-order Møller−Plesset perturbation theory[23] (MP2, frozen core approximation) and the 6-311++G-(2d,2p) basis set.[27] The stationary points were verified as minima by numerically computing the vibrational frequencies using double difference. Other geometries were constructed using various constraints as described in the next section. The restricted Hartree−Fock (RHF) molecular orbitals were localized using the energy localization method due to Edmiston and Ruedenberg.[21] All calculations were performed with the quantum chemistry code GAMESS,[28] and the density difference plots were prepared using the MacMolPlt program.[29]

V. Results and Discussion

A. Structural Details. Fully optimized [MP2/6-311++G-(2d,2p)] structures of H_2O, OH^-, $(H_2O)_2$, and $[HOH\cdots OH]^-$ are shown in Figure 2a−d, respectively. The structures of these hydrogen-bonded systems have been discussed previously[18,19,30,31] and we only note that the monomer structures are perturbed upon complexation. In particular, the O−H bonds directly involved in the hydrogen bonds are lengthened by 0.007 and 0.132 Å for the neutral and anionic species, respectively.

The energies of the complexes displayed in Figure 2c,d relative to the energies of the respective isolated monomers are −5.29 and −28.21 kcal/mol, respectively. The latter energy difference compares favorably with the experimental value of −27 kcal/mol.[31] The difference in hydrogen bond strength ($\Delta\Delta E$) is therefore −22.92 kcal/mol, and the focus of this study is a conceptual understanding of this large increase in hydrogen bond strength.

As is evident from Figure 2, the transformation from a neutral to anionic water dimer changes many intra- and intermolecular parameters that, in addition to the loss of a proton, may play a role in this 22.92 kcal/mol energy decrease. To isolate the primary contribution, we introduce these changes in a stepwise fashion as shown in Scheme 1.

Structures I and V above correspond to the optimized structures of Figure 2c,d, respectively, i.e., $\Delta\Delta E = \Delta\Delta E_{V-I}$. Structure II represents the water dimer structure where the internal geometries of the two water molecules are the optimized structure of isolated water (r_{OH} = 0.958 Å, HOH angle = 104.28°). The remaining degrees of freedom are those of the fully optimized water dimer structure (Figure 2c, $R_{neutral}$ = 2.917 Å). In structure III the OO distance is decreased from that in the neutral water dimer to that of $[HOH\cdots OH]^-$ (R_{anion} = 2.492 Å) and the internal molecular geometries remain those of the isolated monomers (r_{OH} = 0.918 Å) while the *intermolecular* geometry remains that of the optimized water dimer. Structure IV is identical to structure III except that a proton has been removed from the acceptor molecule. Structure V allows full relaxation to the optimized $[HOH\cdots OH]^-$ structure. By keeping the internal monomer geometries fixed to those of the optimized isolated molecules in structures II, III, and IV, the primary electronic effects due to decreasing R and removing the proton, respectively, are separated from each other and from secondary effects due to changes in internal geometry. The associated energy changes are listed in Table 1, together with their internal and intermolecular contributions (cf. eq 15),

$$\begin{aligned}\Delta\Delta E_{X-Y} &= \Delta E_X - \Delta E_Y \\ &= [\Delta E_X(\mathbf{A}) - \Delta E_Y(\mathbf{A})] + [\Delta E_X(\mathbf{D}) - \Delta E_Y(\mathbf{D})] + \\ &\qquad [E_X(\mathbf{A}|\mathbf{D}) - E_Y(\mathbf{A}|\mathbf{D})] \\ &= \Delta\Delta E_{X-Y}(\mathbf{A}) - \Delta\Delta E_{X-Y}(\mathbf{D}) + \Delta E_{X-Y}(\mathbf{A}|\mathbf{D})\end{aligned} \tag{19}$$

The deviation in structure II from the fully optimized minima (structure I) leads to an energy increase of only 0.03 kcal/mol (see Table 1). The change in energy due to the shortening of the OO distance addressed in ΔE_{III-II} and the relaxation of the internal geometries of structure IV as compared to the optimized anion (ΔE_{V-IV}) are both on the order of 5 kcal/mol and offset each other. On balance, these changes account for only a small percentage of the total value of $\Delta\Delta E_{V-I}$ and are significantly smaller than the −23.18 kcal/mol change that occurs when the proton is removed (ΔE_{IV-III}). It is especially interesting to note that the 0.132 Å lengthening of the donating OH bond contributes only 4.35 kcal/mol to the hydrogen bond strength. *This indicates that while a significant lengthening of the donating bond may be indicative of a strong hydrogen bond, it is not primarily responsible for the strength*. This result is not entirely unexpected, since the movement of the proton toward its acceptor in a LBHB should, by definition, have little effect on the total energy. Thus, the remainder of this section will primarily discuss the changes in ΔE obtained upon removing the proton from the acceptor in hydrogen-bonded complex (ΔE_{IV-III}).

The energy analysis is carried out within the conceptual framework pioneered by Ruedenberg.[15,16] The internal energy changes are shown to arise from a competition between *kinetic energy pressure* and *nuclear suction*, while the intermolecular energy changes are semiquantitatively explained in terms of classical electrostatic interactions. Physical insight into these energy changes is facilitated by density difference plots of individual LMOs and the magnitude of electrostatic moments, respectively.

B. $\Delta\Delta E_{III-II}$. In this step the two heavy atoms are brought closer together without changing any other geometrical parameters. The rise in internal energy of both the donor and acceptor as the OO distance is decreased past R_{eq} (see Figure 1) is largely due to a rise in the kinetic energy pressure as described in previous studies.[18−20] The KE of all the valence orbitals on the acceptor and of the bo'_D orbital (see Scheme 2 for MO labels) on the donor increase because the orbital is compressed. The intermolecular energy decreases mainly due to the interaction of bo'_D with lp'_A, but this decrease is dominated by the internal energy increase.

C. $\Delta\Delta E_{IV-III}$. As shown in Table 1, $\Delta\Delta E_{IV-III}$ accounts for the majority (−23.18 kcal/mol) of the total change in binding energy ($\Delta\Delta E$ = −22.92 kcal/mol) observed on going from the fully optimized $(H_2O)_2$ structure to the fully optimized $[HOH\cdots OH]^-$ structure. Step III → IV corresponds to changing the acceptor molecule from H_2O to OH^- *solely* by removing a proton from water. It is easily apparent that the large relative energy decrease in this step is due entirely to the −53.11 kcal/

SCHEME 1

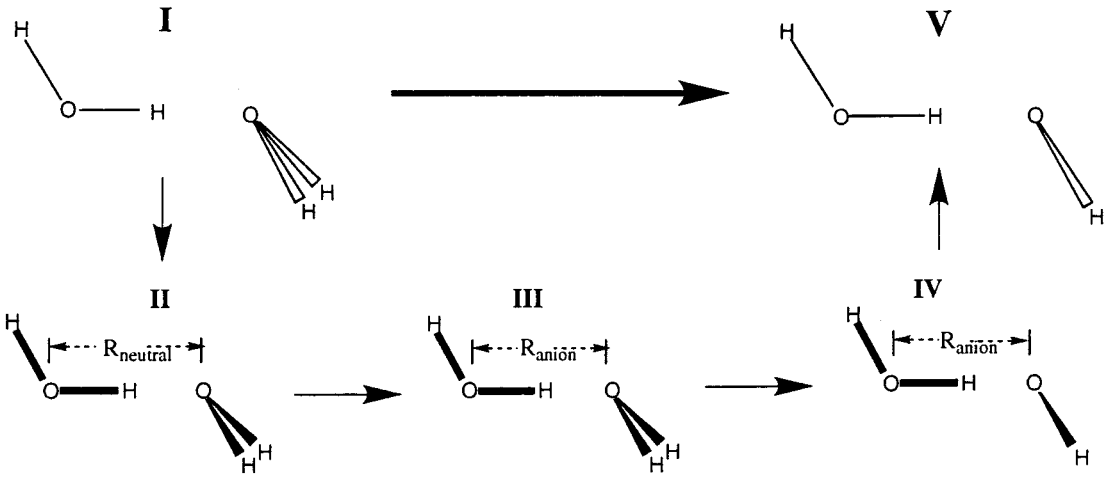

TABLE 1: Values (kcal/mol) for ΔE, $\Delta\Delta E$, and Their Components for Structures I−VI in Scheme 1

	I	II	III	IV	V
E	−5.29	−5.26	−0.68	−23.86	−28.21
E(D)	8.61	8.37	30.08	41.44	75.77
E(A)	11.10	10.82	36.34	54.92	83.18
E(A|D)	−25.01	−24.44	−67.11	−120.22	−187.16
	II−I	**III−II**	**IV−III**	**V−IV**	**V−I**
E	0.03	4.58	−23.18	−4.35	−22.92
E(D)	−0.24	21.71	11.36	34.33	67.16
E(A)	−0.28	25.52	18.58	28.26	72.08
E(A|D)	0.57	−42.67	−53.11	−66.94	−162.15

TABLE 2: Interaction Energies (kcal/mol) between the LCDs in Structures III and IV[a]

$E_{III}(i_A\|j_A)$	co_D	lp'_D	lp_D	lp_D	bo_D	$E_{III}(i_A\|\mathbf{D})$
co_A	−0.01	−0.08	−0.08	−0.04	−0.44	−0.67
lp'_A	−0.60	−16.06	−16.06	−4.61	−37.51	−74.83
lp_A	−0.06	1.34	1.34	−0.32	4.48	6.77
bo_A	−0.03	−0.23	1.36	−0.66	0.37	0.81
bo_A	−0.03	1.36	−0.23	−0.66	0.37	0.81
$E_{IV}(i_A\|j_A)$	co_D	lp'_D	lp_D	lp_D	bo_D	$E_{IV}(i_A\|\mathbf{D})$
co_A	−0.01	−0.09	−0.08	−0.04	−0.44	−0.66
lp'_A	−0.85	−24.50	−27.42	−8.57	−56.27	−117.61
lp_A	−0.08	−1.84	−2.84	0.65	1.04	−3.07
lp_A	−0.07	−3.84	3.55	−1.54	1.02	−0.87
bo_A	−0.06	2.06	−0.43	−0.68	1.10	2.00
$E_{IV-III}(i_A\|j_A)$	co_D	lp'_D	lp_D	lp_D	bo_D	$E_{IV-III}(i_A\|\mathbf{D})$
co_A	0.00	0.00	0.00	0.00	0.00	0.01
lp'_A	−0.26	−8.44	−11.36	−3.96	−18.76	−42.78
lp_A	−0.02	−3.18	−4.18	0.97	−3.44	−9.85
bo_{A/lp_A}	−0.04	−3.61	2.19	−0.87	0.65	−1.68
bo_A	−0.03	0.69	−0.19	−0.01	0.73	1.19

[a] The interaction energies between symmetry equivalent LMOs represent the sum total of all interactions. Note: The last column is the sum of the five previous columns and represents the interaction of a particular LCD on **A** with all the LCDs on **D**.

mol drop in the intermolecular energy:

$$\Delta\Delta E_{IV-III} = \underset{-23.18}{\Delta\Delta E(\mathbf{D})_{IV-III}} + \underset{11.36}{\Delta\Delta E(\mathbf{A})_{IV-III}} + \underset{18.58}{\Delta\Delta E_{IV-III}(\mathbf{A}|\mathbf{D})}$$

$$-53.11 \text{ kcal/mol}$$

This decrease is partially offset by an increase in the internal energies of the monomers. We analyze both of these trends separately.

*1. ΔE_{IV-III} (**A**|**D**).* Table 2 lists the intermolecular energy terms for interactions between the individual LCDs in structures III and IV, labeled in Scheme 2.As expected, LCD contributions involving the accepting lone pair (lp'_A) dominate the intermolecular energies in both structures III (−74.83 kcal/mol) and IV (−117.61 kcal/mol). The −42.78 kcal/mol decrease is mainly due to the attractive interaction of lp'_A with three different LCDs on the donor: the OH bond (bo'_D, −18.76 kcal/mol) and the two lone pairs (lp_D, −19.80 kcal/mol total). Thus, an explanation of the increase in hydrogen bond strength is, to a large extent, reduced to an explanation of the increased interaction between these pairs of LCDs.

SCHEME 2

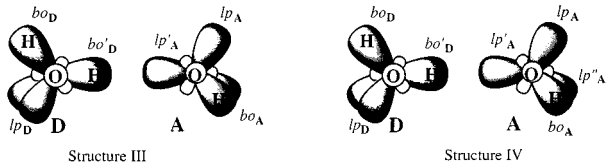

The interaction between bo'_D and lp'_A can be modeled by representing bo'_D by two dipoles, lp'_A in the neutral structure (III) by a single dipole, and lp'_A in the anion (IV) by a dipole as well as a −1/3 point charge located at the acceptor oxygen nucleus (see section II.D for more details).

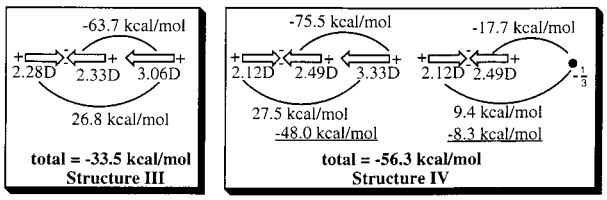

These dipolar and charge-dipolar representations of the LCD interactions compare well with the ab initio LCD values of −37.51 and −56.27 kcal/mol, respectively. On the basis of this analysis we attribute *most* (about two-thirds) of the increased attraction to a more polar lone pair in OH^- compared to H_2O rather than to the net charge in structure IV. A similar analysis of the interactions between lp'_A and the donor lone pairs (lp_D; labeled lp_D and lp'_D in IV) is shown below:

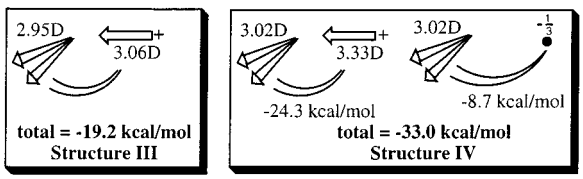

TABLE 3: Changes in the Kinetic, Potential, and Correlation Energies (in kcal/mol) of Individual LCDs for Structures III and IV and Step III → IV in Scheme 1

D LMOs					**A** LMOs				
III	ΔKE	ΔPE	ΔE^{SCF}	ΔE^{MP2}	III	ΔKE	ΔPE	ΔE^{SCF}	ΔE^{MP2}
co_D	−13.13	5.78	−7.35	*a*	co_A	−7.78	3.51	−4.27	*a*
lp_D	−35.95	23.28	−12.67	−0.11	lp'_A	16.84	7.27	24.11	0.61
lp_D	−35.95	23.28	−12.67	−0.11	lp_A	17.29	−15.01	2.28	0.09
bo'_D	134.80	−61.64	73.16	1.15	lp_A	19.31	−12.78	6.53	0.24
bo_D	−27.68	16.46	−11.22	−0.09	bo_A	19.31	−12.78	6.53	0.24
D LMOs					**A** LMOs				
IV	ΔKE	ΔPE	ΔE^{SCF}	ΔE^{MP2}	IV	ΔKE	ΔPE	ΔE^{SCF}	ΔE^{MP2}
co_D	−11.42	4.79	−6.63	*a*	co_A	−16.65	7.75	−8.90	*a*
lp_D	−63.36	43.51	−19.85	−0.31	lp'_A	34.09	6.97	41.06	1.20
lp_D	−58.07	39.80	−18.27	−0.27	lp_A	27.19	−20.64	6.55	0.55
bo'_D	206.44	−95.10	111.33	1.66	lp_A	30.15	−23.16	6.99	0.57
bo_D	−65.67	39.90	−25.77	−0.45	bo_A	29.97	−23.82	6.15	0.76
D LMOs					**A** LMOs				
IV-III	ΔΔKE	ΔΔPE	$\Delta\Delta E^{SCF}$	$\Delta\Delta E^{MP2}$	IV-III	ΔΔKE	ΔΔPE	$\Delta\Delta E^{SCF}$	$\Delta\Delta E^{MP2}$
co_D	1.71	−0.99	0.72	*a*	co_A	−8.87	4.24	−4.62	*a*
lp_D	−27.41	20.23	−7.18	−0.20	lp'_A	17.25	−0.30	16.95	0.59
lp_D	−22.12	16.52	−5.60	−0.15	lp_A	9.90	−5.63	4.27	0.47
bo'_D	71.63	−33.46	38.17	0.51	$bo_{A/lpA}$	10.84	−10.38	0.46	0.33
bo_D	−37.99	23.44	−14.56	−0.36	bo_A	10.66	−11.05	−0.38	0.52

[a] The MP2 correlation energy is calculated using the frozen core approximation.

Though these multipolar representations of the LCD interactions underestimate the magnitude of the ab initio values of 32.12 and 51.92 kcal/mol, the increased attraction is modeled fairly accurately (to within 70%). The charge on the OH^- now contributes more to the energy decrease than the increased polarity, since the two sets of multipoles are further apart and the distance dependence is R^{-2} for the charge−dipole interaction as compared to R^{-3} for the dipole−dipole interaction.

Our qualitative analysis of the LCD interaction energies shows that the increased polarity of the OH^- lone pair is a large part of the reason OH^- is a better hydrogen bond acceptor than H_2O. For the free monomers, the lone pair dipole increases from 2.91D in H_2O to 3.10D in OH^-. This increased polarity is presumably due to the fact that the extra lone pair on OH^- is "shorter" and "fatter" then the corresponding bond in H_2O, which causes expansion of the other lone pairs in OH^- (compared to their H_2O counterparts).

A more quantitative prediction for the lengthening of the OH lone pair dipole can be made by approximating the lone pair LMO as an sp^3 Slater type orbital-hybrid, for which Coulson[32] derived the following expression for the centroid of charge (relative to the origin at the atomic center):

$$\langle r\rangle - R_N = \left(\frac{5}{2}\right)\frac{1}{Z_{\text{eff}}} \tag{20}$$

where Z_{eff} if the effective nuclear charge. On the basis of eq 20 and with Slater's values[33] for the effective nuclear charge of O and O^-, we predict that the lone pair dipole in OH^- is 1.08 times longer than in H_2O:

$$\frac{\mu_{OH^-}(\text{lp})}{\mu_{H_2O}(\text{lp})} \approx \frac{Z_O}{Z_{O^-}} = \frac{4.55}{4.20}$$

which compares well with the actual value of 1.07 (3.10/2.91) for free OH^- and H_2O.

2. $\Delta\Delta E_{IV-III}$***(D)*** *and* $\Delta\Delta E_{IV-III}$***(A)***. The internal energies of the monomers increase on changing the acceptor from H_2O to OH^- and attenuates the increase in hydrogen bond strength. This is not unexpected in light of the fact that lp'_A is expanded in OH^- compared to H_2O (see above) and that the concomitant increase in overlap between lp'_A and bo'_D increases their kinetic energies. This is verified by decomposing the internal monomer energies into kinetic, potential, and correlation energy terms for each orbital. Table 3 reports these values for structures III, IV, and for ΔE_{IV-III}. This decomposition indeed identifies the donating bond (bo'_D) and the accepting long pair (lp'_A) as the main contributors to the internal energy increase of the donor and acceptor, respectively. Furthermore, the kinetic energy increase is responsible for the total energy increase in both LCDs: 17.25 and 71.63 kcal/mol for lp'_A and bo'_D respectively. The origin of these KE increases are discussed next.

In forming structure III from free monomers, the second central moment of lp'_A (a measure of its size) decreases from 3.7258 to 3.6672 au while for structure IV the change is much larger: 4.8111 to 4.5441 au. This can be visualized by comparing the density differences in Figure 3b,d. The inverse relation between the second moment predicts a KE increase for IV that is larger than for III (cf. eq 9):

$$\frac{\text{IV}}{\text{III}} = \frac{(4.5441)^{-1} - (4.8111)^{-1}}{(3.6672)^{-1} - (3.7258)^{-1}} = 2.8$$

This compares reasonably well with the ab initio value of 2.0 (34.09/16.84).

Interestingly, a similar analysis of the relative kinetic energy change in bo'_D predicts a smaller KE change for structure IV than for structure III.

$$\frac{\text{IV}}{\text{III}} = \frac{(3.3187)^{-1} - (3.4429)^{-1}}{(3.2974)^{-1} - (3.4425)^{-1}} = 0.9$$

A comparison of the density difference plots of bo'_D in III and IV (Figure 3a,c) shows the origin of this discrepancy. It is evident that bo'_D in IV is indeed more polarized than in III, but due to the buildup of a tail on the donor in IV the orbital contraction, as measured by $\langle r^2\rangle$, is smaller in IV. However, the larger tail leads to an increase in the gradient of the MO and therefore to a larger increase in the kinetic energy for IV.

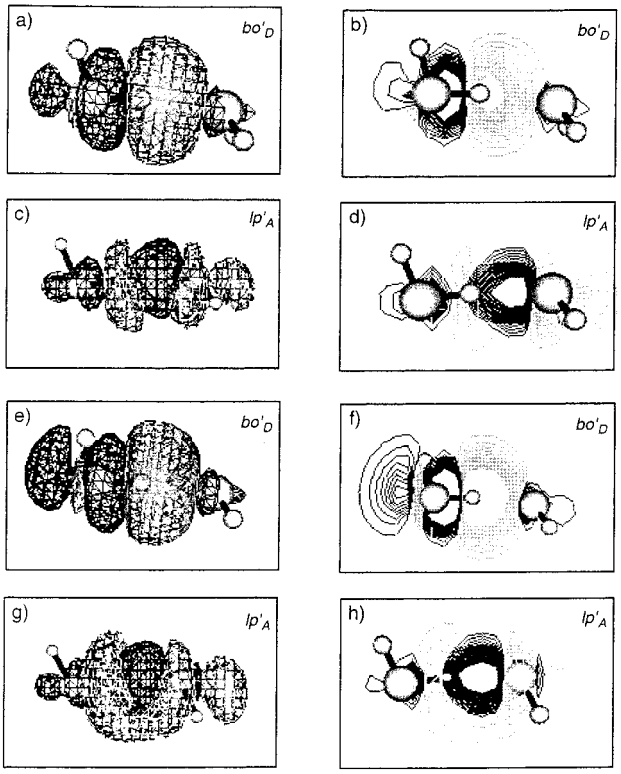

Figure 3. 2D density difference plots for the **D** and **A** LMO most directly involved in the hydrogen bond relative to that of free water for structures III (a−d) and IV (e−h). Light and dark regions refer to a density decrease and increase, respectively. The 3D plots show the 0.00086 e/Bohr^3 isodensity surface. The 2D plots have a maximum contour value of 0.0032 e/Bohr^3 and a contour spacing of 0.0005 Bohr^3. The plotting plane is the molecular plane of **D**.

In summary, the internal energies of both the donor and acceptor increase because the larger lone pair on OH^- results in a larger polarization of the donor bond and the acceptor lone pair directly involved in the hydrogen bond.

D. $\Delta\Delta E_{V-IV}$. The final step Scheme 1 corresponds to a lengthening of the bo'_D bond and a general relaxation of all other geometrical parameters from the free monomer geometries back to the optimized $[HOH\cdots OH]^-$ geometry. As noted previously, the lengthening of this bond increases the hydrogen bond strength by 4.35 kcal/mol and is thus not *primarily* responsible for the large (23.18 kcal/mol) increase in $\Delta\Delta E_{V-I}$. However, as one reviewer noted, a strengthening of a hydrogen bond within an enzyme active site by 4.35 kcal/mol could have a nontrivial effect on the enzyme's catalytic efficiency. In this section we briefly discuss the origin of the 4.35 kcal/mol energy lowering.

1. $\Delta E_{V-IV}(\boldsymbol{A}|\boldsymbol{D})$. The overall energy change in this step is negative because of the large decrease in the intermolecular energy:

$$\underset{-4.35}{\Delta\Delta E_{V-IV}} = \underset{34.33}{\Delta\Delta E_{V-IV}(\mathbf{D})} + \underset{28.26}{\Delta\Delta E_{V-IV}(\mathbf{A})} + \underset{-66.94\ \text{kcal/mol}}{\Delta E_{V-IV}(\mathbf{A}|\mathbf{D})}$$

As in the case of $\Delta\Delta E_{IV-III}$, this decrease is dominated by the interaction between the acceptor lone pair LCD directly involved in the hydrogen bond and two different kinds of LCDs on the donor: the OH bond (bo'_D, −57.98 kcal/mol) and the two lone pairs (lp_D and lp'_D, −11.17 kcal/mol). As before, the origin of these energy decreases are analyzed in terms of multipoles.

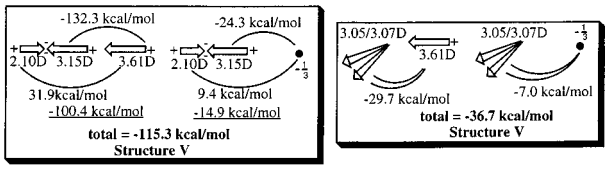

The $lp'_A - bo'_D$ interaction is reproduced surprisingly well using multipoles (the ab initio value is −114.3 kcal/mol), but only 33% of the energy decrease due to lp'_A interacting with lp_D and lp''_D on going from structure IV to structure V can be accounted for by this model. According to this analysis, the lengthening of the donating OH bond increases the polarity of the bond significantly. The analysis shows that the position of the centroid of charge in bo'_D remains approximately fixed relative to the donor O, so that the bond lengthening mainly increases the attractive dipole (from 2.49 to 3.15 D). This increased interaction also elicits a further polarization of the lp'_A dipole (from 3.33 to 3.61 D), which in turn increases the interaction energy with the lone pairs on the donor.

2. $\Delta\Delta E_{V-IV}(\boldsymbol{D})$. The overall energy decrease in this step is small compared to the interaction energy value because the decrease is almost completely balanced by internal energy increases for both the donor and acceptor. A decomposition of the relative internal energy of the donor,

$$\underset{34.34}{\Delta\Delta E_{V-IV}(\mathbf{D})} = \underset{3.69}{\Delta\Delta E_{V-IV}(co_D)} + \underset{64.66}{\Delta\Delta E_{V-IV}(bo'_D)} + \underset{-8.47}{\Delta\Delta E_{V-IV}(bo_D)} + \underset{-12.28}{\Delta\Delta E_{V-IV}(lp'_D)} + \underset{-13.26\ \text{kcal/mol}}{\Delta\Delta E_{V-IV}(lp_D)}$$

makes it clear that the energy increase is driven by the increase in energy of bo'_D. Further decomposition

$$\underset{64.66}{\Delta\Delta E_{V-IV}(bo')} = \underset{-46.16}{\Delta\Delta KE_{V-IV}(bo')} + \underset{109.76}{\Delta\Delta PE_{V-IV}(bo')} + \underset{1.06\ \text{kcal/mol}}{\Delta\Delta E^{(2)}_{V-IV}(bo')}$$

shows that the internal energy increase of bo'_D (63.6 kcal/mol) is due to an increase in the potential energy (109.76 kcal/mol). The kinetic energy decreases (by −46.16 kcal/mol) because the orbital expands along with the bond.

The potential energy term for the bond consists of the potential energy of the bo'_D LCD itself, as well as its interactions with every LCD on the donor:

$$\underset{109.76\ \text{kcal/mol}}{\Delta\Delta PE_{V-IV}(bo'|x)} = \underset{-0.40}{\Delta\Delta PE_{V-IV}(|core)} + \underset{125.50}{\Delta\Delta PE_{V-IV}(|bo')} + \underset{-2.59}{\Delta\Delta PE_{V-IV}(|bo)} + \underset{-6.33}{\Delta\Delta PE_{V-IV}(|lp')} + \underset{-6.43}{\Delta\Delta PE_{V-IV}(|lp)}$$

The main contribution to the energy increase is the energy of bo'_D itself, a result of the loss of attraction between the bonding electron pair and the departing proton (cf. eq 4).

$$\underset{125.5\ \text{kcal/mol}}{\Delta\Delta PE_{V-IV}(bo'_D)} = \underset{15.7}{\Delta\Delta V_{V-IV}(bo'_D|Z_{bo}(O))} + \underset{178.7}{\Delta\Delta V_{V-IV}(bo'_D|Z_{bo}(H))} + \underset{-42.6}{\Delta\Delta g_{V-IV}(bo'_D)} + \underset{-26.4}{\Delta\Delta G_{V-IV}(bo'_D)}$$

Thus, it is this single interaction that is primarily responsible

for the increase in the total internal energy of the donor upon the lengthening of the bond.

3. $\Delta\Delta E_{V-IV}$ ***(A)***. The internal energy increase of the acceptor is a result of the increased energy of all the valence LMOs, but most particularly of lp'_A:

$$\underset{28.26}{\Delta\Delta E_{V-IV}(\mathbf{A})} = \underset{0.24}{\Delta\Delta E_{V-IV}(co_A)} + \underset{12.04}{\Delta\Delta E_{V-IV}(lp'_A)} + \underset{6.87}{\Delta\Delta E_{V-IV}(bo_A)} + \underset{4.32}{\Delta\Delta E_{V-IV}(lp''_A)} + \underset{4.79\ \text{kcal/mol}}{\Delta\Delta E_{V-IV}(lp_A)}$$

For this orbital, kinetic energy decreases (−24.03 kcal/mol) and potential energy increases (35.91 kcal/mol), indicating an expansion of the orbital consistent with the increase in its dipole noted earlier.

In summary, the donating O−H bond lengthens to increase its polarity, which increases the interaction with other orbitals. This increases the internal energy of the monomers significantly, resulting in a relatively small net decrease in the total energy.

E. Other Energy Decomposition Schemes. Many energy decomposition schemes have been applied to hydrogen-bonded systems.[34] Virtually all schemes decompose the total interaction energy into components such as Coulomb interactions, exchange repulsion, charge transfer, and electron density deformation, by calculating the total energy of certain partially optimized wave functions. In contrast, the LCD scheme decomposes the total interaction energy into contributions from localized parts of the fully optimized wave function. However, the different analysis schemes offer similar perspectives. For example, a reduced variational space (RVS) analysis[34e] of $\Delta\Delta E_{IV-III}$ yields Coulomb, exchange repulsion, polarization, and charge-transfer contributions of −20.95, 9.29, −7.93, and −3.59 kcal/mol, respectively. Thus, the increase in hydrogen bond strength is primarily due to an increased Coulomb and polarization energy, which is only partially offset by an increase in the steric (exchange) repulsion energy. The RVS results are thus consistent with the general conclusion reached by using the LCD method. However, further (detailed) information about the chemical origin of these four numbers requires further analysis. The RVS and related methods cannot be used for the analysis of $\Delta\Delta E_{V-IV}$ since the monomer geometries change.

VI. Summary and Future Directions

The increase in hydrogen bond strength on going from HOH···OH_2 to [HOH···OH]$^-$ is analyzed using the theory of localized charge distributions (LCDs, summarized in sections IIA,B), and within the conceptual framework of competing electronic kinetic (KE) and potential energy (PE) pioneered by Ruedenberg. Following a previous study of the water dimer by Jensen and Gordon the interaction energy is divided into an internal energy change of each monomer in the dimer relative to free water, plus an intermolecular energy (eq 5). As the hydrogen bond forms, the internal energy of each monomer must increase since the free monomer represents its variational energy minimum, and the initial decrease in the total energy comes from a decrease in intermolecular energy. The intermolecular energy dominates until the equilibrium separation is reached, at which point the internal energies start to increase faster (Figure 1), and the bond strength is the sum of all three energy values at this point.

The primary structural differences that have been invoked to explain the difference in bond strength between the H_2O···HOH and [HOH···OH]$^-$ include the decreased OO distance, the lengthening of the donating OH bond, and the loss of a proton. By isolating these phenomena, it is shown that the removal of the proton is the most significant factor since it creates a net charge. The net charge itself contributes to an increased intermolecular energy, but it also increases the polarity of the lone pair involved in the hydrogen bond acceptor. The two contributions to the intermolecular energy are roughly equally important. The internal energies of both the donor and acceptor increase because the larger lone pair on OH^- results in a larger polarization of the donor bond and the accepting lone pair upon hydrogen bond formation. However, the change in intermolecular energy is longer range than the change the internal energies. Thus, the OO distance decreases *as a result* until the balance between internal and intermolecular energy is restored (Figure 4). Furthermore, since OH^- is a better acceptor, the energetic benefit of lengthening the HO−H bond to increase its polarity increases *as a result*. However, since the lengthening is accompanied by large increases in the internal energy, it contributes a relatively small amount to the decrease in the total energy.

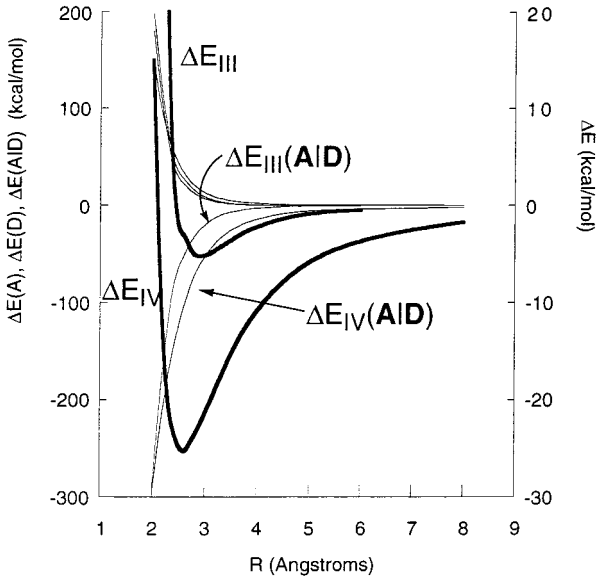

Figure 4. Change in the total (bold, right *y*-axis), internal, and intermolecular energies (eq 15) of $(H_2O)_2$ and [HOH···OH]$^-$ (structures III and IV in Scheme 1) relative to infinite separation and as a function of OO separation.

The conceptual picture that results from our analysis of [HO−H···OH]$^-$ leads to some general conclusions.

For example, replacing OH^- with a molecule that has a longer accepting lone pair dipole (such as NH_2^-), should in principle increase the hydrogen bond strength. In practice, however, the increased attraction will result in proton transfer and a weaker bond since the N−H bond is less polar. Both conclusions have been verified for other molecules in computational experiments by Chen, McAllister, Lee, and Houk.[12] Thus, the pK_a match criterion can be interpreted as an equalization of the dipoles of the proton-accepting lone pairs (assuming all other factors are equal), leading to the best possible intermolecular energy.

However, the bond strength of [HO−H···OH]$^-$ can in principle be increased by replacing OH^- by an acceptor that does not affect the intermolecular energy greatly but reduces the increase in the internal energies in analogy with the findings of Minikis and Jensen[20] for H_2O···HF. Thus, the strongest SSHB [A−H···B]$^-$ is not necessarily that for which the pK_a's are matched since that criterion neglects the steric interaction between A^- and B^-. This neglect can also explain any nonlinear correlation between SSHB strength and ΔpK_a for very (sterically) different acceptors.

Furthermore, the increased strength can be traced to a few electron pairs and is thus a very localized property of the molecule. So, for example, a formal charge rather than a molecular charge may be sufficient to form a SSHB. This is consistent with a recent computational study of $H_3NO\cdots HF$ by Alkorta and Elguero.[35]

Future studies will address these issues.

Acknowledgment. This work was supported in part by the University of Iowa Biosciences Initiative Pilot Grant and a starter grant from the Petroleum Research Fund. The calculations were performed on IBM RS/6000 workstations generously provided by the University of Iowa. The authors thank Daniel Quinn for a careful reading of the manuscript.

References and Notes

(1) Jeffrey, G. *An Introduction to Hydrogen Bonding*; Oxford University Press: New York, 1997.
(2) Cleland, W. W.; Kreevoy, M. M. *Science* **1994**, *264*, 1887.
(3) Gerlt, J. A.; Gassman, P. G. *J. Am. Chem. Soc.* **1993**, *115*, 11552.
(4) Warshel, A.; Papazyan, A.; Kollman, P. *Science* **1995**, *269*, 102.
(5) Warshel, A. *J. Biol. Chem.* **1998**, *273*, 27035.
(6) Scheiner, S.; Kar, T. *J. Am. Chem. Soc.* **1995**, *117*, 6970.
(7) Shan, S.; Loh. S.; Herschlag, D. *Science* **1996**, *272*, 97. (b) Shan, S.; Herschlag, D. *Proc. Natl. Acad. Sci. U.S.A.* **1996**, *93*, 14474.
(8) McAllister, M. A. *Can. J. Chem.* **1997**, *75*, 1195. (b) Pan, Y.; McAllister, M. A. *J. Am. Chem. Soc.* **1998**, *120*, 166.
(9) Mulholland, A. J.; Lyne, P. D.; Karplus, M. *J. Am. Chem. Soc.* **2000**, *122*, 534.
(10) Cleland, W. W.; Frey, P. A.; Gerlt, J. A. *J. Biol. Chem.* **1998**, *273*, 25529.
(11) Kumar, G. A.; McAllister, M. A. *J. Org. Chem.* **1998**, *63*, 6968.
(12) Chen, J. C.; McAllister, M. A.; Lee, J. K.; Houk, K. N. *J. Org. Chem.* **1998**, *63*, 4611.
(13) The authors would be interested to learn of any exceptions.
(14) Experimental data compiled by: Gao, J.; Garner, D. S.; Jorgensen, W. L. *J. Am. Chem. Soc.* **1986**, *108*, 4784.
(15) Ruedenberg, K. *Rev. Mod. Phys.* **1962**, *34*, 326.
(16) Feinberg, M. J.; Ruedenbert, K.; Mehler, E. L. In *Advances in Quantum Chemistry*; Lowdin, P. O., Ed.; Academic Press: New York, 1971; Vol. 5, p 27.
(17) (a) England, W.; Gordon, M. S. *J. Am. Chem. Soc.* **1971**, *93*, 4649. (b) England, W.; Gordon, M. S. *J. Am. Chem. Soc.* **1972**, *94*, 4818. (c) Gordon, M. S.; England, W. *Chem. Phys. Lett.* **1972**, *94*, 5168. (d) Gordon, M. S.; England, W. *Chem. Phys. Lett.* **1972**, *15*, 59. (e) Gordon, M. S.; England, W. *J. Am. Chem. Soc.* **1973**, *95*, 1753. (f) Gordon, M. S. *J. Mol. Struct.* **1974**, *23*, 399 (g) England, W.; Gordon, M. S.; Ruedenberg, K. *Theor. Chim. Acta* **1975**, *37*, 177.
(18) Jensen, J. H.; Gordon, M. S. *J. Phys. Chem.* **1995**, *99*, 8091.
(19) Gordon, M. S.; Jensen, J. H. *Acc. Chem. Res.* **1996**, *29*, 536.
(20) Minikis, R. M.; Jensen, J. H. *Int. J. Quantum Chem.* **2000**, *76*, 341.
(21) (a) Edmiston, C.; Ruedenberg, K. *Rev. Mod. Phys.* **1963**, *35*, 457. (b) Raffenetti, R. C.; Ruedenberg, K.; Janssen, C. L.; Schaefer, H. F., III *Theor. Chim. Acta* **1993**, *86*, 149.
(22) Jensen J. H.; Gordon, M. S. *J. Am. Chem. Soc.* **1995**, *117*, 8159.
(23) Pople, J. A.; Krishnan, R.; Schlegel, H. B.; Binkley, J. S. *Int. J. Quantum Chem. Symp.* **1979**, *13*, 325.
(24) Petersson, G. A.; Al-Laham, M. A. *J. Chem. Phys.* **1991**, *94*, 6081.
(25) Levine, I. N. *Quantum Chemistry*, 3rd ed.; Allyn and Bacon: Boston, 1983; p 402.
(26) Jensen, J. H.; Gordon, M. S. *Mol. Phys.* **1996**, *89*, 1313 and references therein.
(27) Krishnan, R.; Binkley, J. S.; Seeger, R.; Pople, J. A. *J. Chem. Phys.* **1984**, *80*, 3265. (b) Clark, T.; Chandrasekhar, J.; Spitznagel, G. W.; P. von Schleyer, R. *J. Comput. Chem* **1983**, *4*, 294−301. (c) The two d exponents on the non-hydrogen atoms were obtained by multiplying the standard d exponent from the 6-31G(d,p) basis set by 2.0 and 0.5. Likewise for the two p exponents on the hydrogen atoms.
(28) Schmidt, M. S.; Baldridge, K. K.; Boatz, J. A.; Elbert, S. T.; Gordon, M. S.; Jensen, J. H.; Koseki, S.; Matsunaga, N.; Nguyen, K. A.; S. S. T.; Windus, T. L.; Dupuis, M.; Montgomery, J. A. *J. Comput. Chem.* **1993**, *14*, 1347.
(29) Bode, B. M.; Gordon, M. S. *J. Mol. Graphics Modeling* **1999**, *6*, 133. (b) http://www.msg.ameslab.gov/GAMESS/Graphics/MacMolPlt.shtml.
(30) Novoa, J.; Planas, M.; Whangbo, M. H.; Williams, J. M. *Chem. Phys.* **1994**, *186*, 175.
(31) Scheiner, S. *Hydrogen Bonding: A Theoretical Perspective*; Oxford University Press: New York, 1997 (see references therein).
(32) Coulson, C. A. *Rev. Mod. Phys.* **1960**, *32*, 170.
(33) Slater, J. C. *Phys. Rev.* **1930**, *36*, 57.
(34) See for example: (a) Murrell, J. N.; Randic, M.; Williams, D. R. *Proc. R. Soc. (London)* **1965**, *A284*, 566. (b) Morokuma, K. *J. Chem. Phys.* **1971**, *55*, 1236. (c) Kitaura, K.; Morokuma, K. *Int. J. Quantum Chem.* **1976**, *10*, 325. (d) Singh, U. C.; Kollman, P. A. *J. Chem. Phys.* **1985**, *83*, 4033. (e) Stevens, W. J.; Fink, W. H. *Chem. Phys. Lett.* **1987**, *139*, 15. (f) Glendening, E. D.; Streitwieser, A. *J. Chem. Phys.* **1994**, *100*, 2900. (g) Gordon, M. S.; Jensen, J. H. Wave functions and Chemical Bonding: Interpretation. *Encyclopedia of Computational Chemistry*; Wiley: New York, 1998; pp 3198−3214.
(35) Alkorta, I.; Elguero, J. *J. Phys. Chem. A* **1999**, *103*, 272.